research papers

The effect of Cr^{3+} doping on the crystalline perfection and optical properties of zinc tris(thiourea)sulfate, a nonlinear optical material

S. K. Kushwaha, K. K. Maurya, D. Haranath and G. Bhagavannarayana*

National Physical Laboratory, Council of Scientific and Industrial Research, Dr K. S. Krishnan Road, New Delhi 110012, India. Correspondence e-mail: bhagavan@mail.nplindia.ernet.in

A study of the effect of Cr^{3+} doping in zinc tris(thiourea)sulfate (ZTS, a well known nonlinear optical material) single crystals on crystalline perfection and optical properties was carried out. Pure and chromium-doped (1 and 2 mol%) ZTS single crystals were grown by the slow evaporation solution technique. The actual concentration of chromium incorporated into the crystal lattice was found to be different, as evaluated by flame atomic absorption spectroscopy. High-resolution X-ray diffraction (HRXRD) analysis revealed that chromium doping led to the creation of vacancies in the grown single crystals. The photoluminescence emission spectra of pure and doped crystals supported the HRXRD findings. The optical band gap of the single crystals increased as a result of the Cr^{3+} doping, but their transparency in the visible region decreased. The doped crystals exhibited higher linear refractive indices than the pure crystals. The optical dielectric constant (ε), the extinction coefficient (k), the average single-oscillator energy for electronic transitions (E_o) and the oscillator strength (E_d) were evaluated for ZTS single crystals and significant changes were observed in these parameters due to the Cr^{3+} doping.

1. Introduction

Owing to the high speed and ease of production of photons, the area of photonics has become an important field of research in view of the demands of modern society for improved telecommunications, and data retrieval, storage, processing and transmission. The design of devices that utilize photons instead of electrons in the transmission of information has created a need for new materials with unique optical properties (Williams, 1984). Hence, it is useful to synthesize new nonlinear optical (NLO) materials and study their structural, physical, thermal and optical properties. It is also equally important to modify the optical properties of known materials by the incorporation of functional groups or dopants, for tailor-made applications (Bhagavannarayana & Kushwaha, 2010; Moitra & Kar, 2007; Ushasree et al., 1999a; Bhagavannarayana et al., 2008). Zinc tris(thiourea)sulfate {ZTS; $Zn[CS(NH_2)_2]_3 \cdot SO_4$} is a well characterized NLO material in the noncentrosymmetric orthorhombic crystal system and space group $Pca2_1$ (point group $mm2$) (Andreetti et al., 1968). It exhibits a low angular sensitivity and hence is useful for second harmonic generation (SHG), with an efficiency 1.2 times that of potassium dihydrogen phosphate (Marcy et al., 1992). Cadmium doping leads to a higher laser-damage threshold and wider optical transparency for ZTS, and better optical properties have been obtained by mixing of phosphate groups (Venkataramanan et al., 1995; Ushasree et al., 1999b). Our recent studies of ZTS in the presence of some

inorganic and organic dopants have elucidated the enhancement of crystalline perfection, which in turn leads to an improvement in the SHG efficiency (Bhagavannarayana et al., 2006, 2008). Chromium is a photorefractive element and therefore significantly modifies the optical parameters of single crystals (Chah et al., 1997; McMillen et al., 1998). As a result of the inherent advantages in this new field and the continuous miniaturization of device technology based on single crystals, crystalline perfection becomes more and more crucial: to realize the full efficiency of their properties, crystals should be free from defects such as structural grain boundaries (Bhagavannarayana, Budakoti et al., 2005). In the present investigation, the effect of chromium (a photorefractive candidate) doping on the optical properties of ZTS single crystals has been studied for the first time, to the best of our knowledge. Single crystals of pure and Cr-doped ZTS were grown in pure, and in 1 and 2 mol% chromium added, saturated aqueous solutions by the slow evaporation solution technique (SEST). The actual concentration of chromium in the doped ZTS crystals was determined by flame atomic absorption spectroscopy (AAS). The crystalline perfection of both undoped and doped crystals was evaluated by high-resolution X-ray diffraction (HRXRD). The photoluminescence (PL) emission behaviour of the crystals was analysed in order to visualize the formation of the colour centres revealed by the vacancies observed by HRXRD. The transparency, absorption coefficient and optical band-gap were also measured. Wavelength-dependent refractive index (wave-

length dispersion) and optical dielectric characterizations were performed by employing ellipsometry.

2. Experimental

2.1. Crystal growth

Pure ZTS was successfully synthesized in an aqueous medium by taking zinc sulfate heptahydrate and thiourea in a 1:3 stoichiometric ratio, following the process reported in our earlier publication (Bhagavannarayana & Kushwaha, 2010). The resulting product was purified by repeated recrystallization. Saturated aqueous solutions of pure and Cr-doped (by 1 and 2 mol% addition to saturated solutions) ZTS were prepared at 300 K. The crystals were grown by SEST. The growth conditions, such as the temperature and pH of the solutions, were closely monitored. For all the crystals, the experimental conditions were kept identical. Good quality single crystals were harvested from the mother solutions after 20 d and photographs of them are shown in Fig. 1. It can be clearly seen that the pure and 1 mol% doped crystals are quite transparent, whereas the 2 mol% doped crystal is slightly opaque, having a whitish structure inside. The low visual
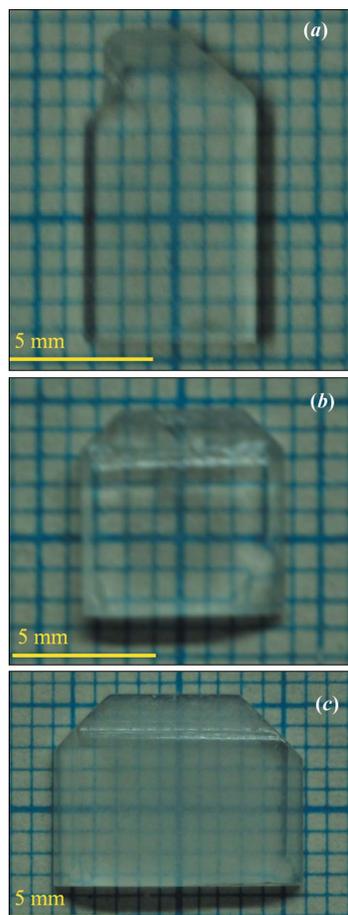

Figure 1
Photographs of (a) pure, (b) 1 mol% and (c) 2 mol% Cr-doped ZTS single crystals.

transparency of the 2 mol% doped crystal may be attributed to the presence of a high concentration of vacancies, as explained in the HRXRD section below.

2.2. Atomic absorption spectroscopy (AAS)

The actual concentration of Cr incorporated into the crystal lattice was determined by AAS (Analytik Jena, Vario-6) with a vapour-generation accessory (AAS-HG). Known quantities of each crystal specimen were dissolved in deionized water and then subjected to analysis.

2.3. Powder X-ray diffraction

The crystal structure and unit-cell parameters of the grown crystals were analysed using a Bruker D8 Advance powder X-ray diffractometer with Cu $K\alpha$ radiation and a graphite monochromator. Diffraction spectra of fine powdered specimens of both pure and doped crystals were recorded in the range $2\theta = 10$–$80°$.

2.4. High-resolution X-ray diffractometry

A PANalytical X'Pert PRO MRD high-resolution XRD system, with Cu $K\alpha_1$ radiation, was employed to assess the crystalline perfection of both pure and doped crystals. The rocking curves of the crystals for the (200) diffraction planes were recorded in symmetrical Bragg geometry using the (100) natural facets by performing an ω scan with triple-axis geometry. The monochromated X-ray beam (Cu $K\alpha_1$) incident on the specimen was obtained using a hybrid two-bounce Ge(220) monochromator with a parabolic multilayer mirror assembly. The diffracted beam from the specimen was detected using a scintillation detector with a triple-axis three-bounce Ge(220) analyser.

2.5. Photoluminescence spectroscopy

The PL emission spectra of the crystals were recorded using a Perkin Elmer LS-55 luminescence spectrometer in the wavelength range 400–700 nm at room temperature. The area of the crystal surface exposed to the incident beam was kept constant for all specimens. A cut-off filter of 390 nm was used to separate out the excitation wavelength from the emission spectra reaching the photomultiplier tube (detector).

2.6. UV–vis–NIR spectroscopy

The UV–vis–NIR transmission and absorption measurements were carried out on a Shimadzu 1601 spectrophotometer in the wavelength range 200–1100 nm. Well polished specimen crystals of the same thickness were used for these studies.

2.7. Ellipsometry

To evaluate the wavelength dispersion behaviour, the extinction coefficient and optical dielectric constants of the pure and doped ZTS single crystals were studied by ellipsometry in the wavelength range 245–1000 nm. The data were recorded for the (100) surfaces.

research papers

3. Results and discussion

3.1. AAS and powder XRD analysis

The concentration of chromium in the doped crystals was evaluated with respect to the elemental composition of pure ZTS. The actual calculated amount of Cr found in the doped single crystals is very much less than the concentration of Cr added to the solution during the growth process. For 1 and 2 mol% doping, the actual amounts of Cr incorporated were found to be 45 and 55 p.p.m., respectively. Powder XRD analysis confirmed the orthorhombic crystal system and space group [$Pca2_1$ (point group $mm2$)] of the grown crystals and no extra phase was observed in the doped crystals (Andreetti *et al.*, 1968). The calculated lattice parameters of the crystals were found to be consistent with previously reported values (Andreetti *et al.*, 1968) and insignificant variation was observed for the doped crystals.

3.2. HRXRD analysis

The recorded HRXRD rocking curves (RCs) for the (200) diffraction planes of the pure and 1 and 2 mol% Cr^{3+}-doped single-crystal specimens are shown in Figs. 2(*a*), 2(*b*) and 2(*c*), respectively. The exact diffraction peak position is taken as zero for all three specimens. In all the RCs, no normalization was made for diffracted intensity. All three RCs have a single peak, which shows that the grown crystals are free from structural grain boundaries (Bhagavannarayana, Ananthamurthy *et al.*, 2005).

The RC of the pure crystal (Fig. 2*a*) is very sharp and its full width at half-maximum (FWHM) is 11″, which is fairly low and close to that expected for an ideally perfect single crystal, according to the plane-wave dynamic theory of X-ray diffraction (Batterman & Cole, 1964). The sharp rise and fall of the diffracted intensity on both sides of the Bragg peak shows that the crystals have a very low density of point defects and their agglomerates (Lal & Bhagavannarayana, 1989). However, on close examination of the RC of the pure crystal one can see that, with respect to the zero peak position, the scattered intensity on the negative side is slightly higher than that on the positive side. Such asymmetry of the RC shows that the pure crystal contains vacancy-type defects. This can be readily understood from the fact that the lattice around a vacancy defect undergoes expansion, leading to an increase in the lattice parameter d, which in turn results in a higher scattering intensity at lower angles with respect to the exact peak position, according to Bragg's law ($2d\sin\theta_B = n\lambda$, where d is the lattice parameter, θ_B is the Bragg angle and λ is the wavelength of the incident X-ray beam). The inset of Fig. 2(*a*) shows a schematic diagram of lattice expansion towards the centre of the vacancy, but only around the defect core.

The RC for the 1 mol% doped crystal (Fig. 2*b*) is quite broad compared with that of the pure crystal. With doping, the FWHM of the RC has increased significantly from 11 to 23″ without any significant asymmetry, which indicates that the doped crystal contains both vacancies and interstitial point defects. The increase in FWHM of the curve may be attributed to the incorporation of chromium in the ZTS crystal lattice.

When the doping concentration is increased to 2 mol%, the FWHM of the RC is further increased to 46″ (Fig. 2*c*). There is now a clear asymmetry in the diffracted intensity with respect to the peak position. This asymmetry in the curve, with higher scattered intensity on the negative side of the peak position, clearly indicates the predominant presence of vacancies in the crystal structure, which may be generated by the incorporation of Cr in the Cr^{3+} ionic state at the substitutional sites of Zn^{2+}. Chromium in general exists in a trivalent state. The ionic radius of Zn^{2+} is 88 pm, and those of Cr^{2+} and Cr^{3+} are 90 and
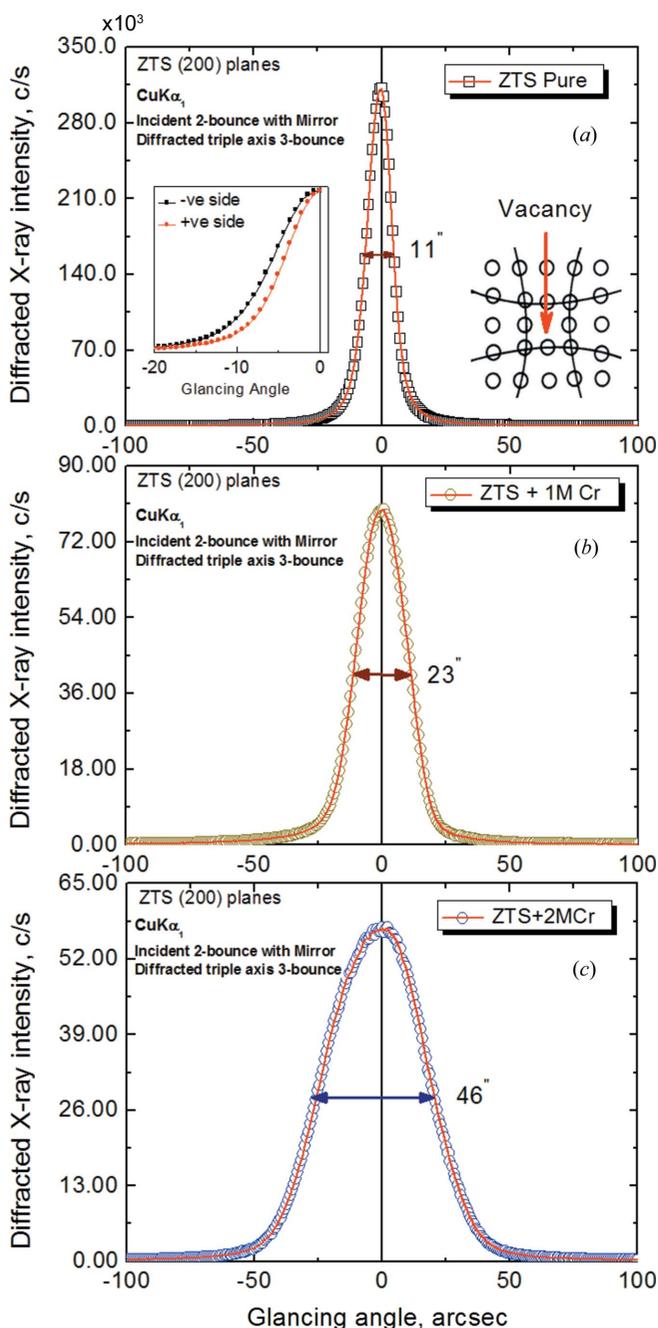

Figure 2
High-resolution XRD rocking curves recorded for the (200) diffraction planes of the ZTS crystals. (*a*) Pure, (*b*) 1 mol% Cr-doped and (*c*) 2 mol% Cr-doped.
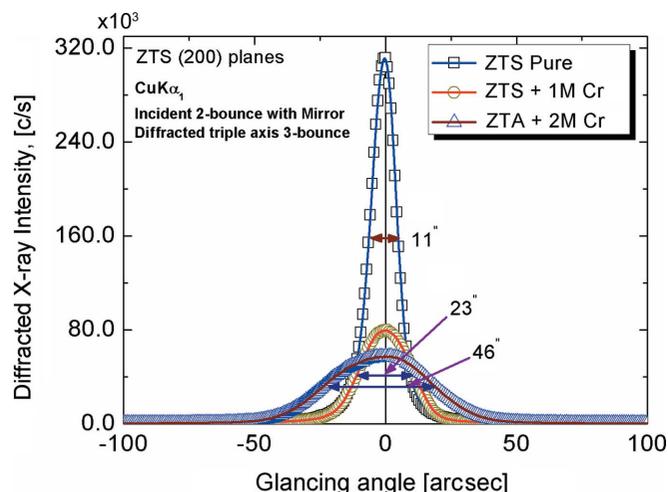
Figure 3
The high-resolution XRD rocking curves of the pure and doped ZTS crystals (of Fig. 2) plotted on a common scale of glancing angle.

75.5 pm, respectively. These values indicate the more ready accommodation of Cr^{3+} than Cr^{2+}, and hence the probability of substitutional occupation by Cr^{3+} is further confirmed. However, because of the requirement for charge neutrality, Cr^{3+} doping in the crystals leads to the formation of vacancies (Xu *et al.*, 2009; Rao & Subramanian, 1980; Meierling, 1971; Bechstein *et al.*, 2009).

Although the FWHM of the RC for 2 mol% doping is almost four times larger than that of the pure crystal, the absence of any extra peak indicates that the Cr^{3+} dopants have been properly accommodated in the host ZTS lattice without leading to any structural grain boundaries. For more insight into the variation in diffracted X-ray intensity or FWHM variation with doping, the RCs for all three specimens are plotted together in Fig. 3. One interesting point in all the curves is that the integrated intensities (*i.e.* the areas under the curves) are more or less the same, which indicates the uniform incorporation of dopants into the crystal structures.
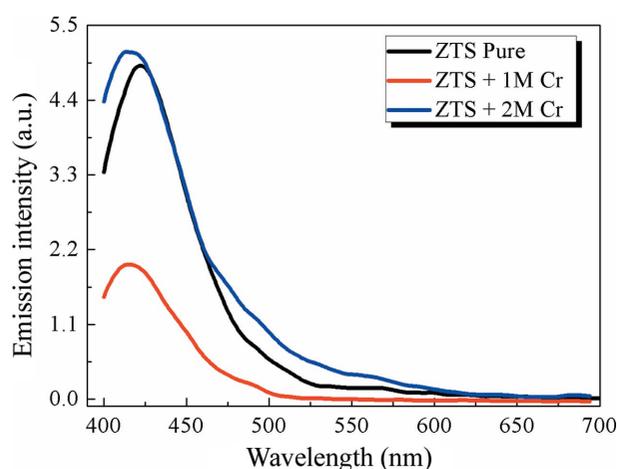
3.3. Photoluminescence analysis

The PL emission spectra for pure and doped ZTS crystals are shown in Fig. 4. The excitation wavelength was 358 nm. The pure crystal shows strong blue emission, peaking at 423 nm. This is attributed to intrinsic vacancy defects present in pure crystals (Xu *et al.*, 1998; Pankratov *et al.*, 2007), which is in agreement with the HRXRD results. With the doping of Cr^{3+} ions (1 mol%) in the ZTS crystal structure, the PL intensity is initially quenched drastically as a result of the 'poisoning effect', as observed with other ions such as Fe, Co, Ni *etc.* (Borse *et al.*, 1999; Rodriguez *et al.*, 2007). In other words, a radiationless redistribution of the excitation energy takes place *via* interaction between the emitting centres and the quenching ions. However, if the doping concentration is increased to 2 mol%, it can be observed that the vacancy-related defects (F-centres) increase predominantly. These act as colour centres and lead the crystal to regain its PL intensity. This is in agreement with the observed HRXRD results, which reveal that the concentration of vacancy defects is very high (Xu *et al.*, 2009), because of the charge-compensation mechanism, in the 2 mol% doped sample. The increased vacancy concentration leads to a considerable enhancement of the PL intensity, as also observed in LiF crystals grown with vacancies (Bhagavannarayana *et al.*, 2011). Interestingly, a slight shift in the PL peak position towards shorter wavelengths is observed upon Cr^{3+} doping of the ZTS crystal, which is anomalous in nature.

3.4. UV–vis–NIR analysis

Transmission spectra for the pure and doped single-crystal specimens are shown in Fig. 5. The spectrum of the pure crystal indicates that it has good transparency over the entire visible region from 300 nm. The transparency of the crystals reduces significantly with Cr^{3+} doping. The slight decrease in transparency of the 1 mol% Cr-doped specimen and the heavy decrease in the 2 mol% Cr-doped specimen may be attributed
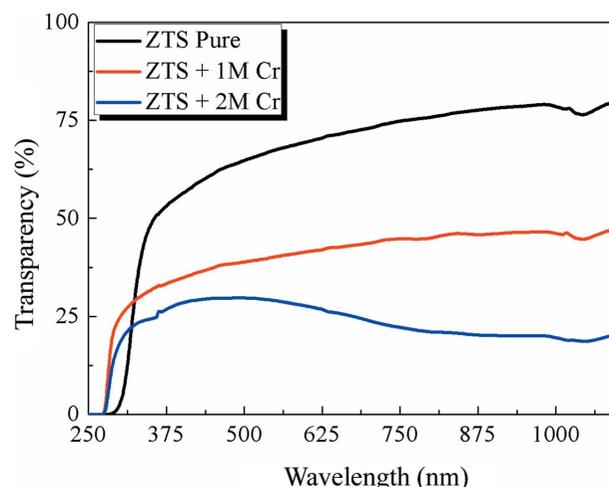

Figure 4
Photoluminescence emission spectra for pure, 1 mol% and 2 mol% Cr-doped ZTS single crystals.

Figure 5
Optical transparency spectra for pure, 1 mol% and 2 mol% Cr-doped ZTS single crystals.

to the existence of a broad absorption band in the visible region due to Cr^{3+} dopants (Bhatt *et al.*, 2003), which leads to the formation of vacancies, as also revealed by HRXRD. The vacancies in the crystal structure generally act as photon-trapping centres and absorb light radiation, leading to poor transparency (Bhagavannarayana *et al.*, 2011). In spite of the decrease in transparency in the visible region, the doped crystals exhibit an enhancement in the transparency range towards the lower wavelengths compared with the pure crystal. Plots of the absorption coefficients (α) *versus* wavelength are shown in Fig. 6(*a*). A blue shift of ~20 nm in the cut-off wavelength is observed for the doped crystals, as can be clearly seen in the inset of the figure. Although the value of α in the UV region is less for the doped crystals than the pure crystal, it is higher over the entire visible region. The optical band gaps of the pure and doped crystals are evaluated using the following relation and plots of $(\alpha h\nu)^2$ *versus* $h\nu$ (Fig. 6*b*):

$$(\alpha h\nu)^2 = A(E_g - h\nu), \tag{1}$$

where α is the absorption coefficient, ν is the frequency of the incident radiation, h is Planck's constant, E_g represents the optical band gap and A is a constant (Ilashchuk *et al.*, 2010). E_g was evaluated by extrapolating the linear part of the plots to the abscissa ($h\nu$), as shown in the figure. The values of E_g for the pure and 1 and 2 mol% doped specimens are 4.34, 4.47 and 4.44 eV, respectively, indicating that the doping has increased E_g considerably. This increase in the band gap is similar to that reported for reduced yttria-stabilized zirconia (PaiVerneker *et al.*, 1989). The widening of E_g for the doped crystals indicates the absence of localized states in the band gap, which might have been present in the pure crystal and obscured the true band gap. Localized states in the band gap generally occur for crystals having extrinsic defects or disorders (Stapper *et al.*, 1999). The slightly higher value for the 1 mol% than the 2 mol% specimen may be attributed to the better perfection of the former. The blue shift observed in §3.3 for the PL peak position may be attributed to the increase in the band-gap energy due to doping.

3.5. Wavelength dispersion analysis

The measured refractive index (RI), n, and extinction coefficient, k, are plotted as a function of wavelength in Fig. 7. The room-temperature linear RI dispersion spectra for the pure and 1 mol% Cr^{3+}-doped crystals are shown in Fig. 7(*a*). We were not able to obtain the values of the refractive index for the 2 mol% doped sample owing to the very low reflected intensity from the crystal surface, which has a high absorbance as observed in the UV–vis analysis. The wavelength-dependent theoretical refractive index values were calculated using Sellmeier's equation:

$$n^2 = A + \frac{B}{\lambda^2 - C} - D\lambda^2, \tag{2}$$

where A, B, C and D are the Sellmeier coefficients with values of 2.8437, 0.0372, 0.0333 and 0.009167, respectively, obtained from the literature (Marcy *et al.*, 1992). Note that the wave-
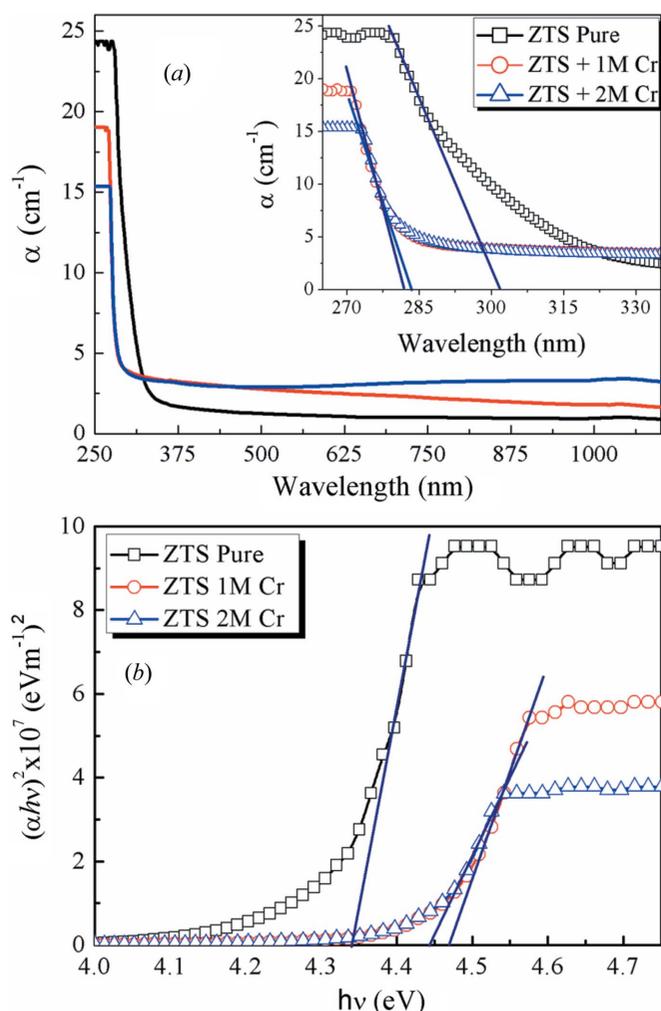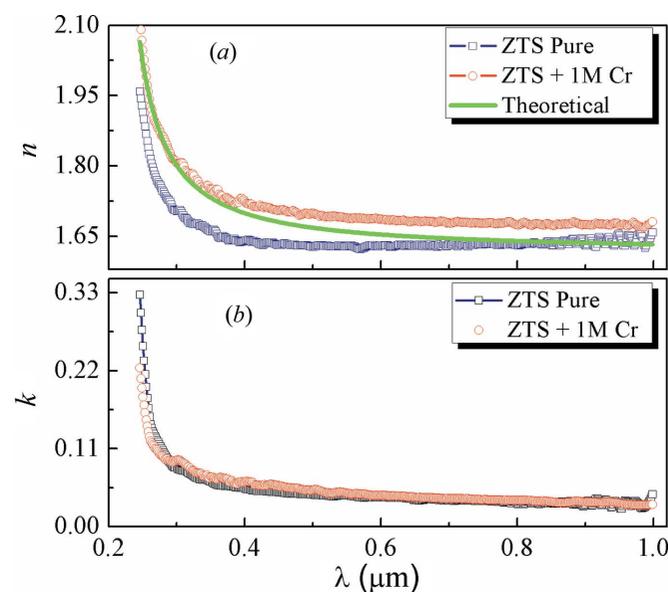

Figure 6
(*a*) Absorption coefficient of pure and doped ZTS single crystals, with an inset showing the blue shift of the cut-off wavelength. (*b*) Showing the increase in band gap of the doped crystals.

Figure 7
(*a*) Linear refracting index and (*b*) extinction coefficient of pure and 1 mol% Cr-doped ZTS single crystals.

Table 1
The theoretically calculated and experimentally obtained linear refractive indices of ZTS single crystals.

	Refractive index		
λ (µm)	ZTS pure	ZTS + 1 mol% Cr	ZTS theoretical
0.245	1.9585	2.0650	2.1144
0.250	1.9140	2.0171	2.0462
0.300	1.7040	1.8011	1.8063
0.351	1.6612	1.7313	1.7504
0.400	1.6403	1.6990	1.7229
0.450	1.6321	1.6803	1.7048
0.501	1.6278	1.6679	1.6986
0.550	1.6284	1.6597	1.6887
0.601	1.6300	1.6534	1.6866
0.650	1.6296	1.6488	1.6821
0.701	1.6338	1.6451	1.6782
0.750	1.6326	1.6422	1.6778
0.801	1.6320	1.6397	1.6735
0.850	1.6320	1.6376	1.6737
0.900	1.6301	1.6357	1.6754
0.950	1.6301	1.6341	1.6731
1.000	1.6300	1.6326	1.6810

length, λ, is here in micrometres. The theoretical RI *versus* λ plot (solid green line) is shown along with the experimental RI plots for the pure and Cr³⁺-doped ZTS crystals. The experimental RI values for both crystals obtained from the ellipsometry analysis follow the same behaviour as the theoretical one. However, compared with the theoretical values, the pure crystal exhibits lower RI values in the lower-wavelength region, although it is well matched at higher wavelengths. For the Cr³⁺-doped crystal, the RI values are well matched to the theoretical values at lower wavelengths, while in the longer-wavelength region they are higher than both the pure and the theoretical data. Both theoretical and experimentally obtained refractive indices, with wavelengths, are given in Table 1. The Cr³⁺ ion is photorefractive in nature and hence significantly modifies the refractive index and other optical properties of host crystals by the electro-optic phenomenon (Chah *et al.*, 1997; McMillen *et al.*, 1998). The extinction coefficients (k) for the pure and doped crystals are plotted with respect to wavelength in Fig. 7(*b*). Both the pure and doped crystals have similar k values over the entire wavelength range.

The linear response of the system to electromagnetic radiation is described by the dielectric function ε. The real (ε_r) and imaginary (ε_i) parts of the optical dielectric constants of the ZTS single crystals are determined using the following relations (Wolaton & Moss, 1963; Wemple, 1977):

$$\varepsilon_r = n^2 - k^2 \quad \text{and} \quad \varepsilon_i = 2nk. \qquad (3)$$

The variations in the real (ε_r) and imaginary (ε_i) parts are shown in Figs. 8(*a*) and 8(*b*), respectively. Both ε_r and ε_i have higher values at lower wavelengths and decrease very fast with increasing wavelength, but for wavelengths above 400 nm they remain almost constant. The ε_r values for the doped specimen are higher over the entire wavelength range, but the ε_i values are almost the same for both crystals. The higher values of ε_r are due to Cr³⁺ doping. The dielectric constant is directly proportional to the polarizability of the crystal, and the

polarizability is related to the valance charge density. The doped Cr³⁺ ions contribute significantly to the polarizability and hence lead to the higher values of ε_r (Groh *et al.*, 2009).

Dispersion plays an important role in research into optical materials, since it is a significant factor in optical communication and in designing devices for spectroscopic dispersion. Single-oscillator parameters are calculated and analysed using the Wemple–DiDomenico model (DiDomenico & Wemple, 1969),

$$n^2 = 1 + \frac{E_d E_o}{E_o^2 - (h\nu)^2}, \qquad (4)$$

where h is Plank's constant, E_o is the average single-oscillator energy for electronic transitions, and E_d is the dispersion energy or oscillator strength, which measures the average strength of interband optical transitions. These parameters for both the pure and the 1 mol% doped ZTS crystals were
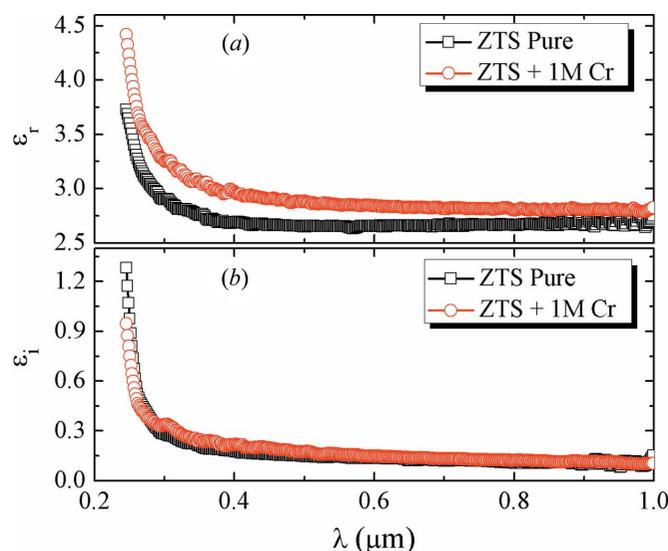

Figure 8
(*a*) Real and (*b*) imaginary optical dielectric constants of pure and 1 mol% Cr-doped ZTS single crystals.
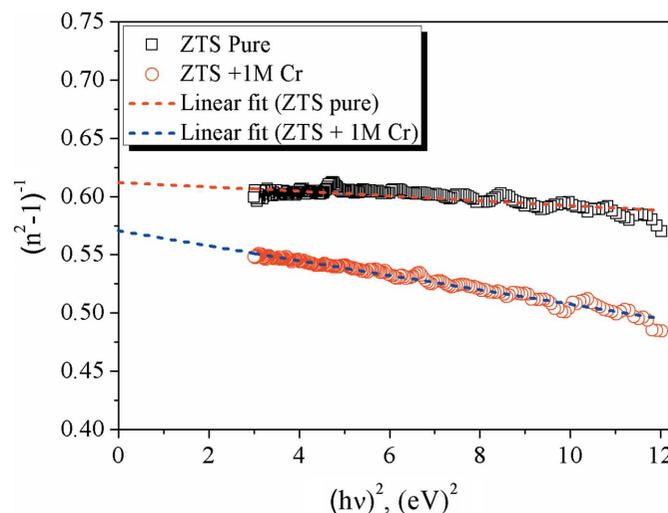

Figure 9
The $(n^2 - 1)^{-1}$ *versus* $(h\nu)^2$ plots for pure and 1 mol% doped ZTS single crystals. The dashed straight lines are the linear fits to the data points.

research papers

Table 2
E_o and E_d parameters for pure and Cr-doped ZTS single crystals.

Specimen	E_o (eV)	E_d (eV)
ZTS pure	17.505	28.563
ZTS + 1 mol% Cr	9.723	17.072

obtained by plotting $1/(n^2 - 1)$ *versus* $(h\nu)^2$ in Fig. 9 for the 3–12 $(eV)^2$ range of $(h\nu)^2$. The plot for the doped crystal indicates a higher slope than that of the pure sample. The dashed red and blue lines are fitted linearly to the data points for the pure and doped crystals, respectively. The E_o and E_d values were calculated from the slope $[(E_o E_d)^{-1}]$ and intercept (E_o/E_d) of the linearly fitted curves in the given energy range, and their values are given in Table 2.

The oscillator strengths and dispersion energies of crystals depend strongly on their structures (Wemple & DiDomenico, 1969). ZTS crystals belong to the space group $Pca2_1$ with $Z = 4$ (Oussaid *et al.*, 2000). The Zn^{2+} ions are tetrahedrally coordinated by three thoiurea S atoms and one sulfate O atom, with all three thiourea molecules nearly coplanar and the S atoms of the thiourea molecule being equidistant from Zn (Venkataramanan *et al.*, 1994). The evaluated E_o and E_d parameters for ZTS fall in the category of tetrahedrally coordinated systems (Wemple & DiDomenico, 1971). The observed lower values of E_o and E_d due to Cr doping may be attributed to Cr^{3+} ions in the lattice of ZTS, which cause the redistribution of electronic charge around these ions and lead to the modification of the spectroscopic properties of the crystals (Ramirez *et al.*, 2004, 2005), and hence the refractive index, by the process of photorefraction (Kushwaha *et al.*, 2011).

4. Conclusions

Pure and chromium-doped single crystals of ZTS have been successfully grown by SEST. The HRXRD analysis revealed that the grown crystals are almost perfect and the incorporated chromium is properly accommodated into the crystalline lattice without leading to the formation of any major defects such as structural grain boundaries. Interestingly, enhanced PL emission intensity was observed at higher doping levels, owing to the formation of vacancies (F-centres), which is in agreement with the HRXRD analysis. The UV–vis optical transparency of the crystals was reduced by a considerable amount for the doped crystals. However, a blue shift in the cut-off wavelength was observed to have taken place. The linear refractive index and the real and imaginary optical dielectric constants have been evaluated. Chromium doping of ZTS crystals leads to an enhancement of the refractive index and makes them suitable for photorefractive applications.

References

Andreetti, G. D., Cavalca, L. & Musatti, A. (1968). *Acta Cryst.* B**24**, 683–690.
Batterman, B. W. & Cole, H. (1964). *Rev. Mod. Phys.* **36**, 681–717.
Bechstein, R., Kitta, M., Schütte, J., Kühnle, A. & Onishi, H. (2009). *J. Phys. Chem. C*, **113**, 3277–3280.
Bhagavannarayana, G., Ananthamurthy, R. V., Budakoti, G. C., Kumar, B. & Bartwal, K. S. (2005). *J. Appl. Cryst.* **38**, 768–771.
Bhagavannarayana, G., Budakoti, G. C., Maurya, K. K. & Kumar, B. (2005). *J. Cryst. Growth*, **282**, 394–401.
Bhagavannarayana, G. & Kushwaha, S. K. (2010). *J. Appl. Cryst.* **43**, 154–162.
Bhagavannarayana, G., Kushwaha, S. K., Shakir, Mohd. & Maurya, K. K. (2011). *J. Appl. Cryst.* **44**, 122–128.
Bhagavannarayana, G., Parthiban, S. & Meenakshisundaram, S. (2006). *J. Appl. Cryst.* **39**, 784–790.
Bhagavannarayana, G., Parthiban, G. & Subbiah, M. (2008). *Cryst. Growth Des.* **8**, 446–451.
Bhatt, R., Kar, S., Bartwal, K. S. & Wadhawan, V. K. (2003). *Solid State Commun.* **127**, 457–462.
Borse, P. H., Deshmukh, N., Shinde, R. F., Date, S. K. & Kulkarni, S. K. (1999). *J. Mater. Sci.* **34**, 6067–6093.
Chah, K., Aillerie, M., Fontana, M. D., Malovichko, G. I., Betzler, K. & Kokanyan, E. (1997). *Opt. Commun.* **136**, 231–234.
DiDomenico, M. & Wemple, S. H. (1969). *J. Appl. Phys.* **40**, 720–734.
Groh, D., Pandey, R., Sahariah, M. B., Amzallag, E., Baraille, I. & Rérat, M. (2009). *J. Phys. Chem. Solids*, **70**, 789–795.
Ilashchuk, M. I., Parfenyuk, O. A., Ulyanytskiy, K. S., Brus, V. V. & Vakhnyak, N. D. (2010). *Semicond. Phys. Quantum Electron. Optoelectron.* **13**, 91–94.
Kushwaha, S. K., Maurya, K. K., Vijayan, N. & Bhagavannarayana, G. (2011). *CrystEngComm*, **13**, 4866–4872.
Lal, K. & Bhagavannarayana, G. (1989). *J. Appl. Cryst.* **22**, 209–215.
Marcy, H. O., Warren, L. F., Webb, M. S., Ebbers, C. A., Velsko, S. P., Kennedy, G. C. & Catella, G. C. (1992). *Appl. Opt.* **31**, 5051–5060.
McMillen, D., Hudson, T. D., Wagner, J. & Singleton, J. (1998). *Opt. Express*, **2**, 491–502.
Meierling, H. D. (1971). *Phys. Status Solidi B*, **43**, 191–197.
Moitra, S. & Kar, T. (2007). *Opt. Mater.* **30**, 508–512.
Oussaid, M., Becker, P. & Carabatos-Nedelec, C. (2000). *Phys. Status Solidi B*, **222**, 553–561.
PaiVerneker, V. R., Petelin, A. N., Crowne, F. J. & Nagle, D. C. (1989). *Phys. Rev. B*, **40**, 8555–8557.
Pankratov, V., Grigorjeva, L., Millers, D. & Yochum, H. M. (2007). *Phys. Status Solidi C*, **4**, 801–804.
Ramírez, M. O., Jaque, D., Bausá, L. E., García Solé, J. & Kaminskii, A. A. (2005). *Phys. Rev. Lett.* **95**, 267401.
Ramirez, M. O., Jaque, D., Montes, M., Garcia Solé, J., Bausá, L. E. & Ivleva, L. (2004). *Appl. Phys. Lett.* **84**, 2787–2789.
Rodriguez, R., Jimenez-Sandoval, S., Estevez, M., Pacheco, S. & Vargas, S. (2007). *J. Sol-Gel Sci. Technol.* **44**, 97–104.
Sambasiva Rao, P. & Subramanian, S. (1980). *Mol. Phys.* **39**, 935–943.
Stapper, G., Bernasconi, M., Nicoloso, N. & Parrinello, M. (1999). *Phys. Rev. B*, **59**, 797–810.
Ushasree, P. M., Jayavel, R. & Ramasamy, P. (1999*a*). *Mater. Chem. Phys.* **61**, 270–274.
Ushasree, P. M., Jayavel, R. & Ramasamy, P. (1999*b*). *Mater. Sci. Eng. B*, **65**, 153–158.
Venkataramanan, V., Srinivasan, M. R. & Bhat, H. L. (1994). *J. Raman Spectr.* **25**, 805–811.

Venkataramanan, V., Subramanian, C. K. & Bhat, H. L. (1995). *J. Appl. Phys.* **77**, 6049–6051.

Wemple, S. H. (1977). *J. Chem. Phys.* **67**, 2151–2168.

Wemple, S. H. & DiDomenico, M. Jr (1969). *Phys. Rev. Lett.* **23**, 1156–1160.

Wemple, S. H. & DiDomenico, M. Jr (1971). *Phys. Rev. B*, **3**, 1338–1351.

Williams, D. J. (1984). *Angew. Chem. Int. Ed. Engl.* **23**, 690–703.

Wolaton, A. K. & Moss, T. S. (1963). *Proc. R. Soc. London*, **81**, 509–513.

Xu, H., Lee, D., Sinnott, S. B., Gopalan, V., Dierolf, V. & Phillpot, S. R. (2009). *Phys. Rev. B*, **80**, 144104.

Xu, S. J., Li, G., Chua, S. J., Wang, X. C. & Wang, W. (1998). *Appl. Phys. Lett.* **72**, 2451–2453.